Nanoscale

PAPER

View Article Online
View Journal | View Issue

Cite this: *Nanoscale*, 2024, **16**, 11211

Structure and vibrational properties of 1D molecular wires: from graphene to graphdiyne†

Francesco De Boni,[a] Roberto Pilot,[a,b] Alberto Milani,[c] Viktoria V. Ivanovskaya,[a] Raichel J. Abraham,[a] Stefano Casalini,[a] Danilo Pedron,[a] Carlo S. Casari,[c] Mauro Sambi[a,b] and Francesco Sedona*[a]

Graphyne- and graphdiyne-like model systems have attracted much attention from many structural, theoretical, and synthetic scientists because of their promising electronic, optical, and mechanical properties, which are crucially affected by the presence, abundance and distribution of triple bonds within the nanostructures. In this work, we performed the two-step bottom-up on-surface synthesis of graphyne- and graphdiyne-based molecular wires on the Au(111). We characterized their structural and chemical properties both *in situ* (UHV conditions) through STM and XPS and *ex situ* (in air) through Raman spectroscopy. By comparing the results with the well-known growth of poly(*p*-phenylene) wires (namely the narrowest armchair graphene nanoribbon), we were able to show how to discriminate different numbers of triple bonds within a molecule or a nanowire also containing phenyl rings. Even if the number of triple bonds can be effectively determined from the main features of STM images and confirmed by fitting the C1s peak in XPS spectra, we obtained the most relevant results from *ex situ* Raman spectroscopy, despite the sub-monolayer amount of molecular wires. The detailed analysis of Raman spectra, combined with density functional theory (DFT) simulations, allowed us to identify the main features related to the presence of isolated (graphyne-like systems) or at least two conjugated triple bonds (graphdiyne-like systems). Moreover, other spectral features can be exploited to understand if the chemical structure of graphyne- and graphdiyne-based nanostructures suffered unwanted reactions. As in the case of sub-monolayer graphene nanoribbons obtained by on-surface synthesis, we demonstrate that Raman spectroscopy can be used for a fast, highly sensitive and non-destructive determination of the properties, the quality and the stability of the graphyine- and graphdiyne-based nanostructures obtained by this highly promising approach.

Received 5th March 2024,
Accepted 15th May 2024

DOI: 10.1039/d4nr00943f

rsc.li/nanoscale

Introduction

Fullerenes,[1] nanotubes,[2] graphene,[3,4] and its derivatives, such as graphene nanoribbons,[5,6] demonstrate that carbon can form a wide variety of structures whose properties are strongly related to structural issues such as dimensionality, hybridization, chirality and topology. Besides carbon nanostructures formed by sp^2- or sp^3-hybridized carbon atoms, there is a great interest in developing carbon nanostructures with a high degree of sp hybridization, because the presence of ethynyl units can considerably affect the conjugation and the properties of carbon-based materials.[7–9] In 1987, Baughman *et al.* first predicted that graphynes (GYs) would be a series of stable 2D crystalline carbon allotropes featuring a high degree of sp hybridization.[10] Since in their structural motif ethynyl units (sp-hybridized carbon) bridge aromatic rings (sp^2–sp^2-hybridised carbon), GYs were named to reflect such arrangements, *i.e.* by recalling graphite and ethyne. Based on the number of triple bonds between two neighbouring aromatic rings, such structures can be distinguished as graphyne (GY, one triple bond), graphdiyne (GDY, two conjugated triple bonds), graphtriyne (GTY, three conjugated triple bonds), and so on. Many efforts, including theoretical predictions and practical experiments, have been made to study GYs during the last few decades, exploring their potential mechanical, optical, and electronic properties. Like in graphene, the existence of Dirac cones was also found in GYs.[11] Moreover, GYs were predicted to have a natural band gap compared with graphene.[12] They also exhibit superior electrical properties: for example, high carrier mobility and small carrier effective masses.[13,14] Thereafter, theoretical studies[15] have predicted interesting

[a]*Dipartimento di Scienze Chimiche, Università degli Studi di Padova, Via Marzolo 1, 35131 Padova, Italy. E-mail: francesco.sedona@unipd.it*
[b]*Consorzio INSTM, Unità di Ricerca di Padova, Padova, Italy*
[c]*Department of Energy, Politecnico di Milano, via Ponzio 34/3, I-20133 Milano, Italy*
†Electronic supplementary information (ESI) available. See DOI: https://doi.org/10.1039/d4nr00943f

electronic,[16,17] optical[18] and mechanical properties[19–21] of GY and GDY for applications in hole-transporting materials,[22] transistors,[23] field emission devices,[24] batteries[25–27] gas separation,[28,29] desalination,[30] catalysis,[31,32] sensors,[33] and electrochemistry.[34] As a general statement, the number and different arrangements of acetylenic moieties play a crucial role in the features of GYs, such as mechanical,[35–37] electronic, and vibrational properties,[38,39] because of long-range changes in conjugation effects.[40,41] A theoretical screening of all the possible GDY structures formed as graphene derivatives has determined 32 different 2D structures, each with specific electronic and vibrational properties.[42,43]

From a synthetic point of view, an appealing approach towards 1D- and 2D-carbon networks containing acetylenic moieties is associated with the so-called on-surface synthesis, namely an ultra-high vacuum (UHV) bottom-up approach that gives access to the synthesis of macrocyclic π-electron systems with atomic accuracy by using designed molecular precursors in combination with modern advances in molecular resolution imaging and represents a unique tool for the realization of novel functional GYs nano-architectures and networks.[44–47] Some of the most promising results have been obtained with the atomically-precise synthesis of graphyne and graphdiyne molecular wires (GY MWs and GDY MWs, respectively), one-dimensional polymers characterized by the presence of phenyl rings and acetylenic moieties within the same wire. Here, we classify these systems according to the following nomenclature: *m*,*n* MWs where *m* is the number of phenyl rings and *n* is the number of alkyne linkages in the repeating monomer (*i.e.* 2,1 and 2,2 MWs are the narrowest GY and GDY nanoribbons, respectively).[48] Up to date, most of the papers reported in the literature exploit linear precursors characterized by terminal alkynes. Unfortunately, this approach leads to defective branched final polymers due to the high reactivity of the terminal alkynes, as well as to the presence, as an intermediate step, of a metallorganic system.[49–53] With reference to the MWs reported in this paper, 2,2 MW were obtained by Rabia, A. *et al.*[38] starting from a precursor featuring the presence of two bromine-terminated triple bonds in *para*-positions of a biphenyl unit. Recently, our group adopted another promising approach based on precursors deposited on silver surfaces wherein the acetylenic moieties are internal rather than terminal, being linked to two phenyl groups, each connecting a bromine atom in *para* position. This choice ensures higher protection of the reactive alkyne chains and allows for direct formation of GY and GDY MW.[54] 2,2 MW were also obtained with this type of precursor by Shan, H. *et al.* starting from and 1,4-di(4-bromophenyl)-1,3-butadiyne (DBPB).[55]

In the field of 2D monolayer materials, and in particular among those obtained by the on-surface synthesis approach, Raman spectroscopy showed high potentiality and low applicability at the same time. Indeed, the technique has limited sensitivity for small quantities of material and enhancement techniques like Surface- or Tip- enhanced Raman scattering are usually required to measure a spectrum.[56,57] A notable exception is constituted by graphene materials, which have a high Raman cross-section and therefore have been widely characterized with this technique. In the field of on-surface synthesis many works on graphene nanoribbons (GNRs) showed that Raman spectroscopy can be used as a fast, non-destructive technique able to determine the width,[58] the edge orientation,[59] the length[60] and the level of alignment[61] of the GNRs. it is also the only technique that can determine the level of defectivity induced by the GNRs transfer procedures.[62]

Only a few works reported the use of Raman spectroscopy on a monolayer of sp-carbon wires produced in ultra-high vacuum (UHV) conditions, which appears challenging due to the scarcity of the analyzed material, to the presence of organometallic species, and to the stability problems affecting the systems when exposed to air conditions.[38,63]

On the other hand, on more bulky materials, Raman spectroscopy is particularly effective in identifying sp/sp^2 hybridization and in investigating the structure, since the principal Raman features of sp-carbon are unique and well-separated from the Raman bands of sp^2 and sp^3 carbon structures.[64–67] Nonetheless, bulky materials tend to be more defective, and the interpretation of the secondary features that are related to the number of the consecutive alkynyl moieties and therefore to the distinction between GY and GDY structures is still challenging.[68,69]

In this work we adopt the afore-mentioned strategy of molecular precursors with phenyl-protected acetylenic moieties. By Ullmann coupling on Au(111), we obtain low defective 2,1 and 2,2 MWs that can be considered as models of the narrowest GY and GDY MWs, respectively. We then compare their structural and vibrational properties with those of the poly(*p*-phenylene) (PPP) MWs (*i.e.* 1,0 MW), which can be considered as the narrowest graphene nanoribbons.[70–72]

The quality of the obtained MWs, confirmed by *in situ* scanning tunneling microscopy (STM) and X-ray photoelectron spectroscopy (XPS), allow us to perform a detailed *ex situ Raman* analysis supported by DFT simulations of the properties of three different sp–sp^2 nanostructures, with particular attention to the main and secondary features that are needed to discriminate the number of triple bonds in the repetitive unit of graphyne- and graphdiyne-based nanostructures.

Despite the scarcity of the material, Raman turns out to be extremely effective in characterizing molecular wires with different sp/sp^2 ratios and provides evidence for their stability in ambient conditions. In this sense, the present work provides a further example, besides those of the graphenic materials, of the great potentiality of Raman spectroscopy in studying carbon nanostructures at the atomic scale, complementing high-resolution STM imaging.

Experimental

All synthesis, STM characterization and XPS spectroscopy were performed in UHV conditions (6×10^{-10} mbar). The single crystal Au(111) surface, provided by MatecK GmbH, was cleaned with several cycles of sputtering with Ar^+ ions at an

energy of 1–1.5 keV for 1 hour at 450 °C, followed by annealing at 550 °C for about 15 minutes. The quality of the surface was monitored by means of STM, XPS, and Low Energy Electron Diffraction (LEED) until an ordered and clean surface was obtained. The organic precursors (purchased from Sigma Aldrich, purity 99%) were sublimated from a pyrolytic boron nitride crucible and deposited on the metallic surface *in situ*. The crucible was held at 120 °C for 4,4″-dibromo-*p*-terphenyl (DBTP) and DBPB, whereas at 60 °C for DBPE precursors. The molecular source was outgassed until the pressure did not increase during the sublimation. During the deposition, the pressure was in the 10^{-9} mbar range, and the substrate was held a few centimeters from the crucible. Then, each sample underwent several steps of annealing for a variable time. The final temperature was kept constant between 2 and 4 hours to allow the system to evolve until it reached a stationary state under the given conditions; the samples were then cooled to RT and characterized *in situ* through STM and XPS, and *ex situ* through Raman spectroscopy.

All STM measurements were performed with an Omicron scanning tunneling microscope (VT-STM) at RT in constant-current mode using electrochemically etched Pt–Ir or W tips. Typical parameters were a tunneling current (I) of 0.5–5 nA and a sample bias voltage (V) of ±1 V referred to the sample (the exact values of current and voltage are reported in the caption of each STM image). The STM images were processed with the WSxM software.[73] Moderate filtering was applied for noise reduction.

DFT calculations have been performed using the OpenMX code.[74,75] The exchange-correlation potential was expressed in the generalized gradient approximation using the Perdew–Burke–Ernzerhof (PBE)[76] schema and dispersion interactions have been included using the Grimme-D2 method.[77] We used norm-conserving fully relativistic pseudopotentials including a partial core correction and a basis set of optimized numerical pseudoatomic orbitals. Charge densities and potentials were determined on a real-space grid with a mesh cutoff energy of 210 Ry. Simulated constant current scanning tunneling microscopy (STM) images have been obtained within the Tersoff–Hamann approximation[78] where the tunneling current is proportional to the local density of surface states at the tip position integrated from the applied voltage bias to the Fermi level.

XPS measurements were performed *in situ* at RT using a VG Scienta XM 650 X-ray source. The X-rays produced were monochromatized using a VG Scienta XM 780 monochromator optimized for Al Kα radiation (1486.7 eV). Photoelectrons were collected at grazing angle emission and analyzed with a Scienta SES 100 electron analyzer fitted to the STM preparation chamber. XPS spectra were fitted with the XPSpeak 4.1 software. Both C 1s and Br 3d peaks are reported with background subtraction in line with our previous analysis[71] this is particularly helpful for Br 3d peaks because is positioned on the shoulder of the Au $5p_{1/2}$ peak.

The Raman measurements of the nanowires were performed in air by using an Ar^+/Kr^+ laser (Coherent, Innova 70) with a beam wavelength of 514.5 nm. The spot size of the laser on the sample was about 5 mm × 80 μm, obtained through a cylindrical lens. The Raman scattering was collected with a camera objective (Canon 50 mm, f/1.2) and it was separated from the elastic scattering by a triple spectrograph (Jobin Yvon S3000). The detector was a charged couple device (CCD), cooled with liquid nitrogen (Jobin Yvon, Symphony). This configuration (macro Raman with line focus) is particularly suitable for delicate and/or low-signal samples.[79] The spectra in the main text were acquired with a laser power of 50 mW, an integration time of 20 seconds and were averaged out of 10 acquisition.

Raman measurements of molecular precursors (in powders) were performed in air in a standard Micro Raman configuration exploiting the same laser source, spectrograph and CCD as before. The laser was coupled into a microscope (Olympus BX 40, Tokyo, Japan) by a non-polarizing beam splitter and focused by a 20x objective (Olympus, LMPlan FLN20x NA = 0.40). The spectra in the main text were acquired with a laser power of 2 mW, an integration time of 10 seconds and were averaged out of 10 acquisition.

The spectra of both polymers and precursors were also collected at different laser powers, to ensure that no sample degradation occurred during measurements (see ESI†).

The simulation of the Raman spectra was carried out on molecular models mimicking the different precursors and on small oligomers obtained by the repetition of 3–4 monomers as models of the polymeric wires. The Au surface is not considered in the Raman simulations. For each molecular wire, two different simulations were performed: the first one assumed a fully planar conformation of the polymers on the surfaces, while the second one added a tilt of about 30° among adjacent repetitive units within the polymers to take into account the steric hindrance between adjacent phenyl rings (ESI Fig. S19–S21†). The DFT simulations of Raman spectra have been carried out by using the Gaussian09 package[80] at the PBE0/cc-pVTZ level of theory: indeed, this combination already proved to provide reliable and accurate predictions of the spectroscopic results for a large variety of sp-based molecular systems.[58,81] When comparing theoretical and experimental Raman spectra, a frequency scaling factor of 0.93 and a shift of +48 cm^{-1} has been applied to the computed ones. This correction has been determined separately by the comparison of the experimental and DFT-computed Raman spectra of the three different molecular precursors and are the scaling factors required to bring the band predicted by the simulations for the vibration modes localized on the phenyl ring and on the triple bond, respectively, near to the experimental 1585 cm^{-1} and 2220 cm^{-1} bands.

Results and discussion

STM and XPS characterization: structural and chemical properties

We performed the synthesis of 2,1 2,2 and 1,0 MW supported on Au(111) starting from different precursors: 1,2-di(4-bromo-

phenyl)-ethyne (DBPE); 1,4-di(4-bromophenyl)-1,3-butadiyne (DBPB) and 4,4″-dibromo-*p*-terphenyl (DBTP), respectively, according to the synthetic route summarized in Scheme 1. After the room temperature (RT) deposition on the gold surface and the subsequent annealing at 170 °C, we obtained long polymeric nanowires, *i.e.* the annealing triggers the release of bromine atoms and the formation of new C–C bonds between adjacent phenyl moieties to produce the final structure of molecular wires, according to the scheme of the well-known on-surface Ullmann-like coupling reaction.

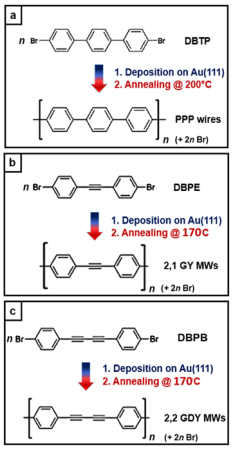

Scheme 1 Representation of the bottom-up growth of different molecular wires on the Au(111) surface: (a) poly-*p*-phenylene (PPP) wires starting from the 4,4″-dibromo-*p*-terphenyl (DBTP) precursor; (b) 2,1 graphyne molecular wires (2,1 MWs) from the 1,2-di(4-bromophenyl)-ethyne (DBPE) precursor; (c) 2,2 graphdiyne molecular wires (2,2 MWs) from the 1,4-di(4-bromophenyl)-1,3-butadiyne (DBPB) precursor.

Fig. 1b, c, f and g report STM images of the molecular wires obtained after the annealing at 170 °C. The small-scale images (b) and (f) show a contrast modulation that is in line with the alternation between phenyl rings (light) and acetylenic groups (dark) within each wire. Indeed, the dark part in the 2,1 MWs repeating monomer is shorter than the same one in 2,2 MWs, in agreement with the presence of a single alkynyl moiety group in the first case and a butadiynyl in the second one.

Complemental DFT simulations can provide a more precise description at the atomic level of the supramolecular organization when compared to STM images. Fig. 1a and e show structural models for both the molecular wires adsorbed at the metal surface. In accordance with experimental images, the polymeric chains have been aligned with the Au[1 − 10] direction. The lattice mismatch is minimized by accommodating a 2,1 MWs monomer over 4 gold surface periods, while for the 2,2 MWs this condition is satisfied for 5 gold surface periods. Both models predict a distance between adjacent chains equal to 7.7 Å, which is in line with the experimental value that is on average 7.5 ± 0.5 Å, whereas the calculated distance from the

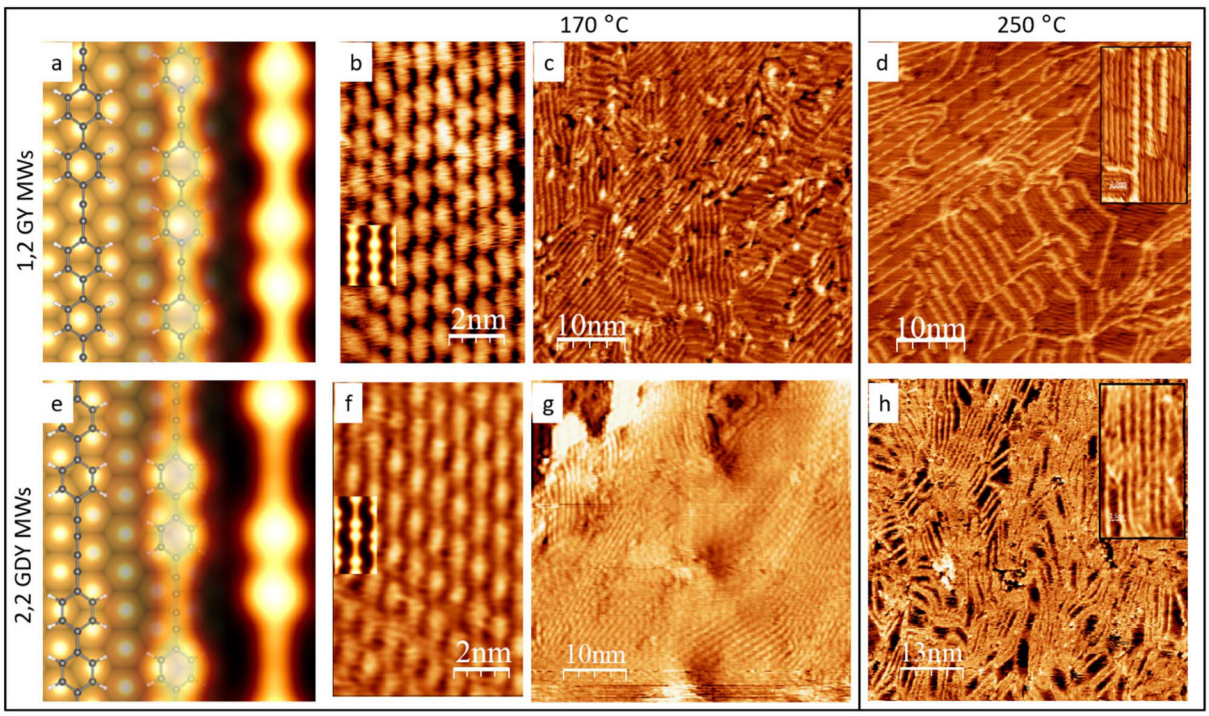

Fig. 1 (a) DFT simulated model and (b) and (c) experimental STM images of 2,1 MWs after annealing the surface at 170 °C; in (b) the DFT-simulated STM image is superimposed to the experimental data. (d) The surface with 2,1 MWs after the thermal treatment at 250 °C, high resolution as inset. (e) DFT simulated model and (f) and (g) STM images of 2,2 MWs after annealing the surface at 170 °C; in (f) the DFT-simulated STM image is superimposed. (h) The surface with 2,2 MWs after thermal treatment at 250 °C, high resolution as inset. (b) 1.9 nA, 0.7 V; (c) 0.8 nA, 1.6 V; (d) 0.9 nA, 1.0 V (f) 1.0 nA 0.9 V (g) 0.8 nA −1.6 V (h) 1.4 nA 1.3 V The ball-and-stick models follow this legend: C atoms – dark grey; H atoms – white; Br atoms – red.

metal surface is 3.6 Å. Adjacent polymers are shifted in the direction parallel to the chains to minimize the repulsion between the phenyl rings. Altogether, the 2,1 MWs supramolecular organization can be fairly described by using a [3 0 0 4] commensurate supercell and the 2,2 MWs superstructure requires a [3 0 0 5] commensurate supercell. Simulated STM images are reported in Fig. 1b and f: the good agreement obtained with the experimental images validates this structural model.

Fig. 1(c) and (g) show larger-scale STM images, which confirm that the surface is fully covered by a monolayer of molecular wires. The degree of order and length of the 2,1 and 2,2 MWs is not comparable with those obtained for PPP wires from DBTP molecules on the same surface, where isooriented MWs longer than 100 nm are easily found (see ESI. Fig. S1†).[54] This is in line with the high reactivity of the triple bond, which can start reacting even after the mild annealing necessary to the debromination, thereby causing branch coupling reactions. Yet, we find that the MWs length is in line with or better than that reported in literature for similar systems.[47] Comparing the average lengths of the two types of molecular wires reported in this paper, we find that the longer ones have been obtained for the 2,2 MWs where 50 nm long wires are easily visualized, whereas the 2,1 MWs are generally shorter, showing, on average, a length of approximately 10 nm and forming many small domains wherein they are oriented along different directions, as evident in Fig. 1c. The same stability trend has been found after a second annealing performed at 250° C for 2 hours, as reported in Fig. 1c and f. While in the case of 2,2 MWs, the polymers are still intact and organized in wavy bundles (Fig. 1h), in the case of 2,1 MWs the surface has completely changed: only a few short bright original polymers are still intact, while most of them have been substituted by darker wires that don not show a clear repetition motif, as evident in Fig. 1d and its inset. We can anticipate that from the Raman spectra analysis, we found that the darker wires come from the degradation of 2,1 MWs caused by the annealing at 250 °C. In the ESI , we report STM images of the MWs obtained by annealing at 170 °C and exposed to air condition for 24 hours, (ESI Fig. S22†) both the STM images and the Raman measurements confirm the stability of MWs within this time frame.

Further information on the reaction sequence as a function of temperature is provided by XPS measurements, reported in Fig. 2 and 3 for the synthesis of 2,1 and 2,2 MWs, respectively.

At RT, the C 1s peak related to DBPE molecules can be fitted with three components: the main peak at 284.0 eV is attributed to sp^2 C–H and sp alkynes carbon atoms (red), the sp^2 C atoms directly linked to other three C atoms (blue) are responsible for the binding energy (BE) component at 284.4 eV, whereas the C atoms directly linked to bromine (green) are responsible for the high BE component at 284.8 eV (Fig. 2a). The attribution of these convoluted peaks is consistent with the results reported previously in the literature.[82–84] The relative areas of these three peaks are in good agreement (within 4%) with the amount of the three carbon species present in the intact molecule (C–H : C–C : C–Br = 10 : 2 : 2), as also reported in Table S2 of ESI.† Moreover, the position of the Br 3d peak (Fig. 2b) is consistent with the non-dissociative

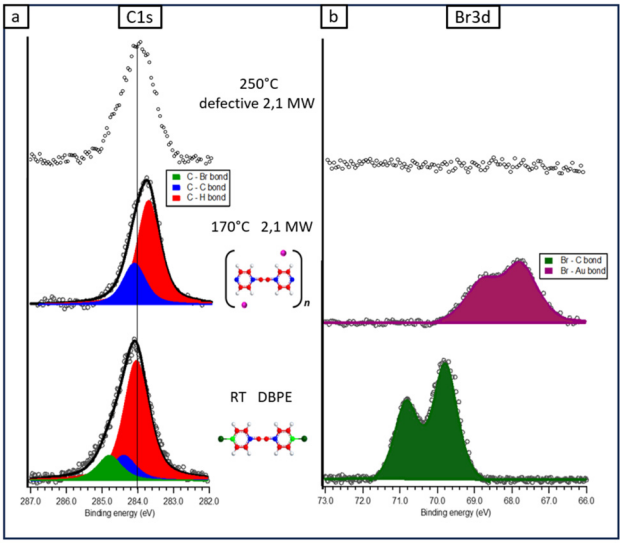

Fig. 2 (a) C 1s and (b) Br 3d XPS spectra for the two-step synthesis of 2,1 MWs from the DBPE precursor on Au(111). In the central panel, C atoms in the different nanostructures are coloured according to the following colour legend: C bonded to Br – light green; C bonded to H – red; C bonded exclusively to C – blue. Instead, Br atoms are represented with the following colour legend: Br bonded to C – dark green; Br chemisorbed on Au – violet.

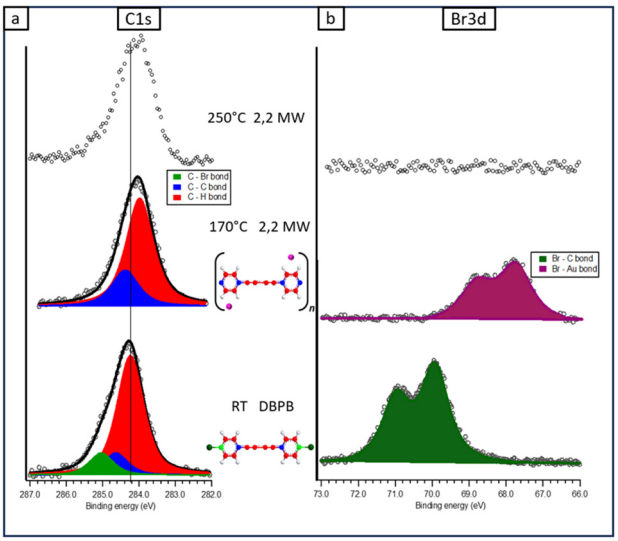

Fig. 3 (a) C 1s and (b) Br 3d XPS spectra for the two-step synthesis of 2,2 MWs from the DBPB precursor on Au(111). In the central panel, C atoms in the different nanostructures are coloured according to the following colour legend: C bonded to Br – light green; C bonded to H – red; C bonded exclusively to C – blue. Instead, Br atoms are represented with the following colour legend: Br bonded to C – dark green; Br chemisorbed on Au – violet.

adsorption of DBPE molecules (Br $3d_{5/2}$ at BE = 69.9 eV), as already observed for similar halogenated precursors;[63,85] *i.e.*, bromine is still bonded to the rest of the molecule rather than being chemisorbed onto gold atoms of the surface.

Similar considerations can be pointed out for the fitting of the C 1s peak of the DBPB molecule (Fig. 3a), except for two main differences. First, a slight increase of BE (about 0.2 eV, see Table S3†) of all three components in the DBPB molecule compared to the corresponding ones in DBPE is detected. Second, there is a different percentage of the abundance of the three carbon species. In fact, the red component increases by about 20% compared to the other two components, reflecting the presence of two more sp-carbon atoms in the structure of the DBPB molecule, so that the relative amount of the three species is now C–H : C–C : C–Br = 12 : 2 : 2.

The formation of the 2,1 MWs modifies the C atoms bonded to bromine into C atoms linked to three C atoms (Fig. 2a): the resulting XPS region can now be fitted with just two components, the red one (BE = 283.7 eV), and the blue one (284.1 eV), with a percentage area compatible with the presence of the graphyne-like molecular wires (C–H : C–C = 10 : 4). These two components show a shift (0.3 eV) toward lower BE with respect to the previous growth step, as extensively confirmed after this stage on many surfaces as a consequence of the bromine adsorption on the metal surface,[63] and the related change in the surface work function.[86] The absence of a component due to C–Br bonds and the total conversion of DBPE into 2,1 MWs is further confirmed by the Br 3d spectrum (Fig. 2b), which shows an important shift toward lower BE (Br $3d_{5/2}$ at 67.9 eV; Fig. 2b), typical of bromine chemisorbed on both gold and other metal surfaces. Moreover, a significant quantity of bromine desorbed, in fact, the area of the Br 3d peak decreased by about one-third compared to the same area at RT. This view holds also for the fitting of the C1s feature of 2,2 MWs, except for the two main differences previously observed. First, the BE of the two C1s components in 2,2 MWs is still about 0.2 eV higher compared to the corresponding ones in 2,1 MWs: such a small increase can probably be attributed to a different interaction with the substrate of the two analyzed MWs. Second, the relative amount of red and blue components reflects, within 3%, the abundance of the two carbon species in the 2,2 MW monomer, *i.e.* C–H : C–C = 12 : 4.

Similar considerations can be pointed out for the two-step growth of PPP wires starting from the DBTP precursor, because this synthesis is already well-known in the literature, hence we report STM images and XPS spectra in the ESI (Fig. S1, S2 and Table S4†).

Regarding the XPS spectra registered after the annealing at 250° C (upper part of Fig. 2 and 3 and corresponding to STM images reported in Fig. 1(d) and (h)), it is important to note that in both cases the Br signal is not detected, in line with its total desorption from the metal surface, within the sensitivity of the technique. Regarding the C1s signal of the 2,2 MW, the shape and intensity remain unchanged with respect to the previous annealing step, whereas in the case of the 2,1 MW, we found a peak with similar intensity but with the FWHM increased by about 20% with respect to the previous annealing step (see Table S1 in ESI† for the parameters). Therefore, the C1s peak confirms what was already reported when analyzing the STM images: the 2,1 MWs degraded after the annealing at 250 °C.

Raman spectroscopy: vibrational properties

As described in the introduction, we exploited the potentialities of Raman spectroscopy in studying the atomic-scale structure of carbon molecular wires based on $sp–sp^2$ hybridization, complementing high-resolution STM imaging. Indeed, by exploiting the high stability of the studied systems, we performed an *ex situ* Raman characterization of the precursor molecules and both 2,1, and 2,2 PPP MWs. To provide a reliable interpretation of the experimental trends, several simulations on the precursor molecules and molecular models were performed for describing the final molecular wires grown on the substrate (see Experimental section for more information).

Fig. 4 reports experimental Raman spectra of DBTP, DBPE and DBPB molecular precursors in powder form before sublimation and their corresponding simulated spectra. The comparison between the experimental and simulated data shows a good agreement of both positions and intensities of the peaks, demonstrating the accuracy of the adopted level of theory. The Raman spectra of the three precursors show important similarities of the peaks related to the phenyl groups (evidenced by yellow lines in Fig. 6), the most important being the signal around 1580 cm^{-1}, attributed to C–C stretching modes localized on the phenyl groups, and other three less intense peaks around 1010 cm^{-1}, 1070 cm^{-1} and 1480 cm^{-1}, with normal modes mainly localized on the two external parts of the molecules (phenyl rings an C–Br bond), and therefore not substantially affected by the presence of triple bonds.

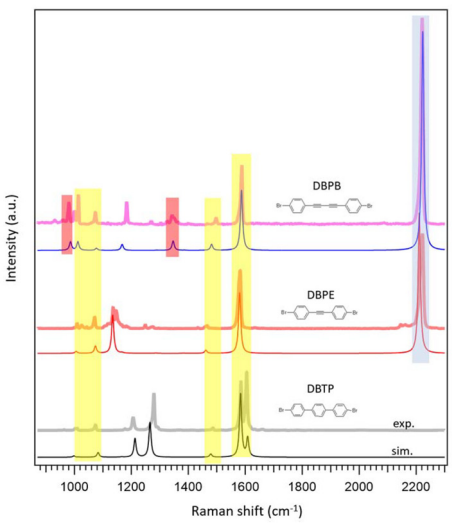

Fig. 4 Experimental (exp.) and simulated (sim.) Raman spectra of the three precursor molecules. A model of each molecule is sketched on the right side of the image, the coloured bars are used to outline differences and similarities between the spectra (see main text).

More interesting is to analyze the differences between the spectra due to the normal modes that involve the central part of the molecules. The most relevant feature is the intense peak around 2220 cm^{-1}, which is associated with the C–C stretching mode of the triple bonds, as reported in Fig. 5a and b. This is the most intense peak in the DBPE and DBPB spectra (blue line in Fig. 4), and it is absent in the DBTP spectrum. Moreover, the Raman spectrum of DBPB molecules shows two minor peaks at 980 cm^{-1} and 1340 cm^{-1} (red lines in Fig. 4) that arise from the stretching of single C–C bonds between the two triple bonds, as visible from the representation of the normal modes shown in Fig. 5c and d and that are not present in the spectrum of DBPE molecules. These peaks can be therefore considered as a fingerprint of the butadiyne group in sp–sp^2 carbon nanostructures.[63,87] All the details about the most significant Raman features of each spectrum are reported in the ESI,† namely experimental and computed wavenumbers, computed Raman intensities, and sketches of the normal modes of vibration.

Fig. 6 reports the *ex situ* Raman spectra of the UHV-synthesized molecular wires after thermal treatment at 170 °C and the comparison with the simulated data. First of all, it is important to stress that the samples prepared for the Raman analysis consist of only one single layer of polymer, as reported in the STM image of Fig. 1. The quality of the Raman spectra is excellent, even though there is a tiny amount of the material of interest. To the best of our knowledge, Raman related to one monolayer thick materials without the help of surface or tip enhancement is reported only for graphenic materials and for the GDY system in the works by Rabia *et al.*[38,63]

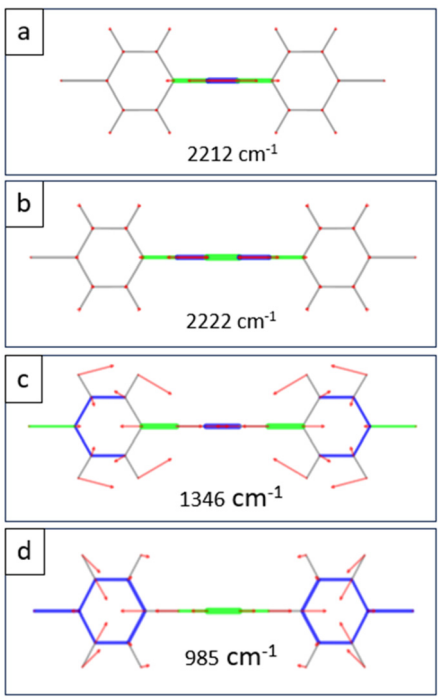

Fig. 5 Sketches of the simulated normal modes of vibration and corresponding wavelength values discussed in the main text for the DBPE (a) and DBPB (b), (c) and (d) molecules. Movements of the atoms are represented according to the following legend: red arrows represent bond bending, while coloured segments show bond stretching with different vibrational phases depending on the colour. The length of the arrows and the width of the segments are proportional to the contribution of each vibration to the whole normal mode.

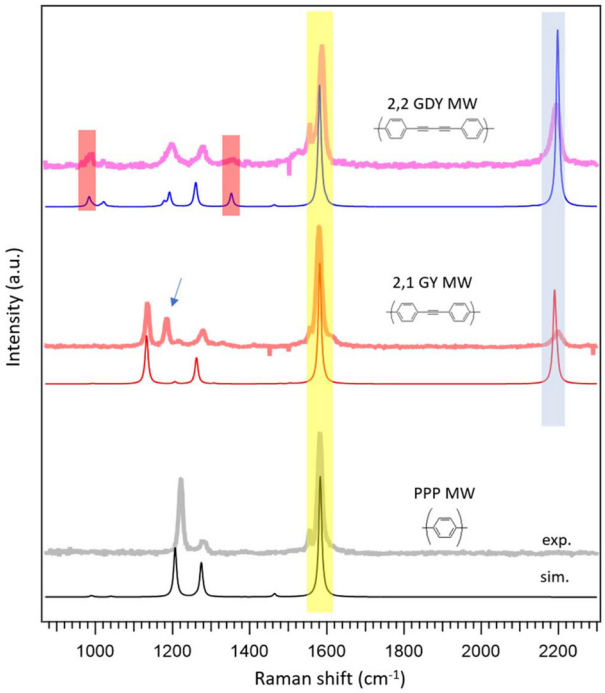

Fig. 6 Experimental (exp.) and simulated (sim.) Raman spectra of the three molecular wires are considered in this work. A model of each monomer is sketched on the right side of the image, the coloured bars are used to outline differences and similarities between the spectra (see main text).

The spectra reported in Fig. 6 highlight the peculiar characteristics already described for the precursor molecules, but some further important aspects must be consider.

The MWs spectra have fewer Raman features compared to the corresponding precursors due to the greater simplicity of the repetitive motif unit and the consequent decrease of the number of normal modes, but the main features are maintained and therefore in Fig. 6 we keep the same colour code employed for the precursors.

Thanks to the agreement between experimental spectra and simulations, we are able to outline the main peaks related to the phenyl rings common to the three MWs with yellow lines, whereas blue lines indicate the peaks related to the triple bonds and red lines those that can be considered the fingerprint of butadiyne groups (Fig. 6). The simulated spectra reported in Fig. 6 are calculated for the fully planar conformations because they fit better with the corresponding experimental spectrum than the tilted models (Fig. S19–S21†).

It is interesting to analyze the main difference between the experimental Raman spectrum of 2,1 MWs and the corresponding simulation in more detail: the peak related to the

triple bond (2205 cm^{-1}) is rather small with respect to the simulated reference and, above all there is a peak at 1185 cm^{-1}, which is not predicted by the simulation (arrow in Fig. 6). An analysis of the Raman literature on similar polymers shows that this peak is characteristic of poly(*p*-phenylene vinylene) (PPV), a polymer characterized by the presence of alternating phenyl rings and double bonds.[88] It is also interesting to analyze the Raman spectrum of the 2,1 MWs after annealing at 250 °C, as reported in Fig. 7. In this case, the peak related to the triple bond at 2205 cm^{-1} completely disappears, whereas the peak at 1185 cm^{-1} increases its intensity. The result is a spectrum perfectly superimposable to that reported for PPV.[88] This is a clear indication that 2,1 MWs tend to react through triple bond breaking (decrease of 2205 cm^{-1} peak) switching from sp to sp^2 hybridization (increase of 1185 cm^{-1} peak).

The elucidation of the mechanism of this reaction is beyond the scope of this paper, but it is quite surprising that 2,2 MWs, which have two consecutive triple bonds, *i.e.* they should be more exposed to side reactions compared to 2,1 MWs, do not produce the peak around 1185 cm^{-1} even after the annealing at 250 °C. Concerning this behaviour, the paper by Shan, H. *et al.*[55], by using AFM atomically resolved images and DFT simulations, evidenced the presence of gold adatoms that act as effective protecting groups for butadiyne units by forming Au–π ligand bonds, preventing unwanted branched coupling reactions.

Raman spectra of 2,2 MWs on Au(111) have been also published by Rabia *et al.*[38] In this case the peak related to the butadiyne group is not visible and the peak of the triple bond at a high Raman shift shows a second component related to the interaction with the substrate, not so evident in our spectra. The reason for the difference is probably related to the different synthetic strategies to obtain the same MWs. The precursor used by Rabia *et al.* features the presence of the two bromine-terminated triple bonds in *para*-positions of a biphenyl unit. This precursor gives rise to the formation of an organometallic intermediate that probably increases the interaction with the substrate, whereas with our precursor this intermediate is not detected.

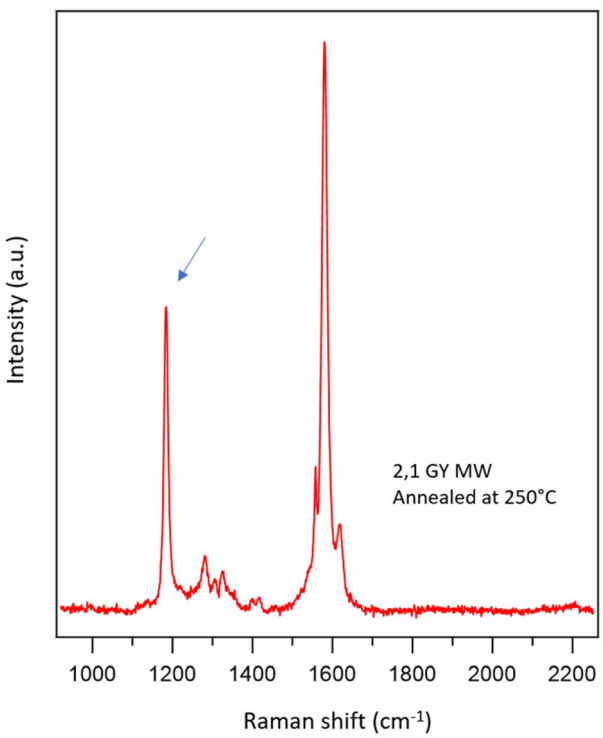

Fig. 7 Experimental Raman spectrum of the 2,1 MWs after annealing at 250 °C.

Conclusions

In this work, we performed the two-step bottom-up growth of long-range ordered graphyne- and graphdiyne-based molecular wires on Au(111) starting from DBPE and DBPB as molecular precursors, respectively. Furthermore, we fully characterized their structural and chemical properties both *in situ* (UHV conditions) through STM and XPS complemented by DFT simulations and *ex situ* (in the air) through Raman spectroscopy. In particular, by also comparing each synthetic step with the well-known growth of PPP wires from the DBTP precursor, we were able to discriminate different numbers of triple bonds in the structure of a molecule or of a repetitive monomeric unit within a nanowire containing phenyl rings. Even if the number of triple bonds can be effectively determined from the main features of STM images and the fitting of C1s peak in XPS spectra, we obtained the most relevant results from Raman spectroscopy. First, this technique provides an important *ex situ* characterization tool, that can be exploited also closer to conditions of the possible applications of this kind of nanostructures. Second, the detailed analysis of Raman spectra, combined with DFT simulations, allowed us to identify the main features related to the presence of two conjugated triple bonds in a row (graphdiyne-like systems), as distinct from those arising from one triple bond (graphyne-like systems).

Moreover, the Raman analysis, in addition to confirming the different high-temperature stability of the MWs, provides clear indications of which functional groups are involved in their thermal degradation and on their reactions, which are difficult to obtain from the standard UHV analysis.

To conclude, this work provides both several powerful strategies to identify the number of triple bonds in graphyne- and graphdiyne-based nanostructures and a full *in situ* and *ex situ* characterization of three different types of such nanostructures.

Conflicts of interest

There are no conflicts to declare.

Acknowledgements

Founded by Italian Ministry of Education, Universities, and Research through the projects “Nanochemistry for Energy and

Health, NexuS" and "Complessità Chimica C^2"—the national funding network termed "Dipartimenti di Eccellenza" awarded to the Department of Chemical Sciences at the University of Padua. M.S acknowledges the financial support of European Union's Horizon 2020 research and innovation programme under the Marie Sklodowska-Curie grant agreement No. 842694. F.S. acknowledges the financial support of European Union - Next Generation EU, DM 351/2022 - PNRR CUP C96E22000410007 and the University of Padova through grant P-DISC#09BIRD2019-UNIPD SMOW. S. C. acknowledges the financial support of the University of Padova through grant P-DiSC#11NexuS_BIRD2020-UNIPD (CARBON-FET).

References

1 F. Diederich and C. Thilgen, Covalent Fullerene Chemistry, *Science*, 1996, **271**, 317–324.
2 A. D. Franklin, Electronics: The Road to Carbon Nanotube Transistors, *Nature*, 2013, **498**, 443–444.
3 A. K. Geim and K. S. Novoselov, The Rise of Graphene, *Nat. Mater.*, 2007, **6**, 183–191.
4 M. Inagaki and F. Y. Kang, Graphene Derivatives: Graphane, Fluorographene, Graphene Oxide, Graphyne and Graphdiyne, *J. Mater. Chem. A*, 2014, **2**, 13193–13206.
5 F. Schwierz, Graphene Transistors, *Nat. Nanotechnol.*, 2010, **5**(7), 487–496.
6 P. B. Bennett, Z. Pedramrazi, A. Madani, Y.-C. Chen, D. G. de Oteyza, C. Chen, F. R. Fischer, M. F. Crommie and J. Bokor, Bottom-up Graphene Nanoribbon Field-Effect Transistors, *Appl. Phys. Lett.*, 2013, **103**(25), 253114.
7 A. L. Ivanovskii, Graphynes and Graphdyines, *Prog. Solid State Chem.*, 2013, **41**, 1–19.
8 N. V. R. Nulakani and V. Subramanian, A Theoretical Study on the Design, Structure, and Electronic Properties of Novel Forms of Graphynes, *J. Phys. Chem. C*, 2016, **120**, 15153–15161.
9 C. Huang, Y. Li, N. Wang, Y. Xue, Z. Zuo, H. Liu and Y. Li, Progress in Research into 2D Graphdiyne-Based, *Mater. Chem. Rev.*, 2018, **118**, 7744–7803.
10 R. H. Baughman, H. Eckhardt and M. Kertesz, Structure-Property Predictions for New Planar Forms of Carbon: Layered Phases Containing sp2 and sp Atoms, *J. Chem. Phys.*, 1987, **87**, 6687–6699.
11 D. Malko, C. Neiss and A. Gorling, Two-Dimensional Materials with Dirac cones: Graphynes Containing Heteroatoms, *Phys. Rev. B: Condens. Matter Mater. Phys.*, 2012, **86**, 045443.
12 M. S. Hybertsen and S. G. Louie, Electron Correlation in Semiconductors and Insulators: Band Gaps and Quasiparticle Energies, *Phys. Rev. B: Condens. Matter Mater. Phys.*, 1986, **34**, 5390–5413.
13 N. Narita, S. Nagai, S. Suzuki and K. Nakao, Optimized Geometries and Electronic Structures of Graphyne and Its Family, *Phys. Rev. B: Condens. Matter Mater. Phys.*, 1998, **58**, 11009–11014.
14 J. M. Chen, J. Y. Xi, D. Wang and Z. G. Shuai, Carrier Mobility in Graphyne Should Be Even Larger than That in Graphene: A Theoretical Prediction, *J. Phys. Chem. Lett.*, 2013, **4**, 1443–1448.
15 Z. Chen, C. Molina-Jiron, S. Klyatskaya, F. Klappenberger and M. Ruben, 1D and 2D Graphdiynes: Recent Advances on the Synthesisat Interfaces and Potential Nanotechnological Applications, *Ann. Phys.*, 2017, **529**, 1700056.
16 G. Luo, X. Qian, H. Liu, R. Qin, J. Zhou, L. Li, Z. Gao, E. Wang, W.-N. Mei, J. Lu, Y. Li and S. Nagase, Quasiparticle Energies and Excitonic Effects of the Two-Dimensional Carbon Allotrope Graphdiyne: Theory and Experiment, *Phys. Rev. B: Condens. Matter Mater. Phys.*, 2011, **84**, 075439.
17 K. Srinivasu and S. K. Ghosh, Transition Metal Decorated Graphyne: An Efficient Catalyst for Oxygen Reduction Reaction, *J. Phys. Chem. C*, 2012, **116**, 5951–5956.
18 J. Wang, S. Zhang, J. Zhou, R. Liu, R. Du, H. Xu, Z. Liu, J. Zhang and Z. Liu, Identifying sp–sp^2 carbon materials by Raman and infrared spectroscopies, *Phys. Chem. Chem. Phys.*, 2014, **16**, 11303–11309.
19 Y. Pei, Mechanical Properties of Graphdiyne Sheet, *Phys. B*, 2012, **407**, 4436–4439.
20 M. Becton, L. Zhang and X. Wang, Mechanics of Graphyne Crumpling, *Phys. Chem. Chem. Phys.*, 2014, **16**, 18233–18240.
21 R. E. Roman and S. W. Cranford, Post-modified Strategies of Graphdiyne for Electrochemical Applications, *Adv. Eng. Mater.*, 2014, **16**, 862–871.
22 S. Jalili, F. Houshmand and J. Schofield, Study of Carrier Mobility of Tubular and Planar Graphdiyne, *Appl. Phys. A*, 2015, **119**, 571–579.
23 Y. Pan, Y. Wang, L. Wang, H. Zhong, R. Quhe, Z. Ni, M. Ye, W. N. Mei, J. Shi, W. Guo, J. Yang and J. Lu, Graphdiyne–Metal Contacts and Graphdiyne Transistors, *Nanoscale*, 2015, **7**, 2116–2127.
24 J. Gong, Y. Tang and P. Yang, Investigation on Field Emission Properties of Graphdiyne–BN Composite, *J. Mol. Struct.*, 2014, **1064**, 32–36.
25 F. Wang, Z. Zuo, L. Li, F. He and Y. Li, Graphdiyne Nanostructure for High-Performance Lithium-Sulfur Batteries, *Nano Energy*, 2020, **68**, 104307.
26 J. He, N. Wang, Z. Cui, H. Du, L. Fu, C. Huang, Z. Yang, X. Shen, Y. Yi, Z. Tu and Y. Li, Hydrogen Substituted Graphdiyne as Carbon-Rich Flexible Electrode for Lithium and Sodium Ion Batteries, *Nat. Commun.*, 2017, **8**, 1172.
27 J. Li, Y. Yi, X. Zuo, B. Hu, Z. Xiao, R. Lian, Y. Kong, L. Tong, R. Shao, J. Sun and J. Zhang, Graphdiyne/Graphene/Graphdiyne Sandwiched Carbonaceous Anode for Potassium-Ion Batteries, *ACS Nano*, 2022, **16**, 3163–3172.
28 Y. Jiao, A. Du, S. C. Smith, Z. Zhu and S. Z. Qiao, H_2 Purification by Functionalized Graphdiyne – Role Of Nitrogen Doping, *J. Mater. Chem. A*, 2015, **3**, 6767–6771.
29 X. Tan, L. Kou, H. A. Tahini and S. C. Smith, Graphynes: Indispensable Nanoporous Architectures in Carbon Flatland, *Mol. Simul.*, 2015, **42**, 573–579.

30 J. Kou, X. Zhou, H. Lu, F. Wu and J. Fan, Graphyne as the Membrane for Water Desalination, *Nanoscale*, 2014, **6**, 1865–1870.
31 J. Kou, X. Zhou, H. Lu, F. Wu and J. Fan, Graphyne as the Membrane for Water Desalination, *Nanoscale*, 2014, **6**, 1865–1870.
32 Z. Lu, S. Li, P. Lv, C. He, D. Ma and Z. Yang, First principles study on the interfacial properties of NM/graphdiyne (NM = Pd, Pt, Rh and Ir): The Implications for NM growing, *Appl. Surf. Sci.*, 2016, **360**, 1–7.
33 X. Chen, P. Gao, L. Guo and S. Zhang, Graphdiyne as a Promising Material for Detecting Amino Acids, *Sci. Rep.*, 2015, **5**, 16720.
34 L. Gao, Z. Yang, X. Li and C. Huang, Post-modified Strategies of Graphdiyne for Electrochemical Applications, *Chem. – Asian J.*, 2021, **16**, 2185–2194.
35 S. W. Cranford and M. J. Buehler, Mechanical Properties of Graphyne, *Carbon*, 2011, **49**, 4111–4121.
36 S. W. Cranford and M. J. Buehler, Selective Hydrogen Purification Through Graphdiyne Under Ambient Temperature and Pressure, *Nanoscale*, 2012, **4**, 4587–4593.
37 Y. Y. Zhang, Q. X. Pei and C. M. Wang, Mechanical Properties of Graphynes Under Tension: A Molecular Dynamics Study, *Appl. Phys. Lett.*, 2012, **101**, 081909.
38 A. Rabia, F. Tumino, A. Milani, V. Russo, A. Li Bassi, S. Achilli, G. Fratesi, G. Onida, N. Manini, Q. Sun, W. Hu and C. S. Casari, Scanning Tunneling Microscopy and Raman Spectroscopy of Polymeric Sp-Sp2 Carbon Atomic Wires Synthesized on the Au (111) Surface, *Nanoscale*, 2019, **11**, 18191.
39 C. S. Casari, M. Tommasini, R. R. Tykwinski and A. Milani, Carbon-atom wires: 1-D systems with tunable properties, *Nanoscale*, 2016, **8**, 4414.
40 P. Serafini, A. Milani, M. Tommasini, C. E. Bottani and C. S. Casari, Topology-Dependent Conjugation Effects in Graphdiyne Molecular Fragments, *Carbon*, 2021, **180**, 265–273.
41 A. Milani, V. Barbieri, A. Facibeni, V. Russo, A. L. Bassi, A. Lucotti, M. Tommasini, M. D. Tzirakis, F. Diederich and C. S. Casari, Structure Modulated Charge Transfer in Carbon Atomic Wires, *Sci. Rep.*, 2019, **9**, 1648.
42 P. Serafini, A. Milani, M. Tommasini, C. Castiglioni, D. M. Proserpio, C. E. Bottani and C. S. Casari, Vibrational Properties of Graphdiynes as 2D Carbon Materials Beyond Graphene, *Phys. Chem. Chem. Phys.*, 2022, **24**, 10524–10536.
43 P. Serafini, A. Milani, D. M. Proserpio and C. S. Casari, Designing all Graphdiyne Materials as Graphene Derivatives: Topologically Driven Modulation of Electronic Properties, *J. Phys. Chem. C*, 2021, **33**, 18456–18466.
44 Y. Li, J. He and H. Shen, Journey from Small-Molecule Diyne Structures to 2D Graphdiyne: Synthetic Strategies, *Chem. – Eur. J.*, 2020, **26**, 12310–12321.
45 F. Kang and W. Xu, On-Surface Synthesis of One-Dimensional Carbon-Based Nanostructures via C–X and C–H Activation Reactions, *ChemPhysChem*, 2019, **20**, 2251.
46 J. Liu, Q.-W. Chen and K. Wu, On-Surface Construction of Low-Dimensional Nanostructures with Terminal Alkynes: Linking Strategies and Controlling Methodologies, *Chem. Lett.*, 2017, **28**, 1631.
47 F. Klappenberger, Y. Q. Zhang, J. Björk, S. Klyatskaya, M. Ruben and J. V. Barth, On-Surface Synthesis of Carbon-Based Scaffolds and Nanomaterials Using Terminal Alkynes, *Acc. Chem. Res.*, 2015, **48**, 2140.
48 X. Li, H. Zhang and L. Chi, On-Surface Synthesis of Graphyne-Based Nanostructures, *Adv. Mater.*, 2019, **31**, 1804087.
49 B. Cirera, Y.-Q. Zhang, J. Björk, S. Klyatskaya, Z. Chen, M. Ruben, J. V. Barth and F. Klappenberger, Synthesis of Extended Graphdiyne Wires by Vicinal Surface Templating, *Nano Lett.*, 2014, **14**, 1891.
50 F. Klappenberger, R. Hellwig, P. Du, T. Paintner, M. Uphoff, L. Zhang, T. Lin, A. B. Moghanaki, M. Paszkiewicz, I. Vobornik, J. Fujii, O. Fuhr, Y.-Q. Zhang, F. Allegretti, M. Ruben and J. V. Barth, Functionalied Graphdiyne Nanowires: On-Surface Synthesis and Assessment of Band Structure, Flexibility, and Information Storage Potential, *Small*, 2018, **14**, 1704321.
51 J. Liu, Q. Chen, L. Xiao, J. Shang, X. Zhou, Y. Zhang, Y. Wang, X. Shao, J. Li, W. Chen, G. Q. Xu, H. Tang, D. Zhao and K. Wu, Lattice-Directed Formation of Covalent and Organometallic Molecular Wires by Terminal Alkynes on Ag Surfaces, *ACS Nano*, 2015, **6**, 6305.
52 Q. Sun, L. Cai, H. Ma, C. Yuan and W. Xu, Dehalogenative Homocoupling of Terminal Alkynyl Bromides on Au(111): Incorporation of Acetylenic Scaffolding into Surface Nanostructures, *ACS Nano*, 2016, **10**, 7023.
53 C. H. Shu, M. X. Liu, Z. Q. Zha, J. L. Pan, S. Z. Zhang, Y. L. Xie and P. N. Liu, On-Surface Synthesis of Poly (p-Phenylene Ethynylene) Molecular Wires via in situ Formation of Carbon-Carbon Triple Bond, *Nat. Commun.*, 2018, **9**, 2322.
54 F. Sedona, M. M. S. Fakhrabadi, S. Carlotto, E. Mohebbi, F. De Boni, S. Casalini, M. Casarin and M. Sambi, On-Surface Synthesis of Extended Linear Graphyne Molecular Wires By Protecting The Alkynyl Group, *Phys. Chem. Chem. Phys.*, 2020, **22**, 12180–12186.
55 H. Shan, Y. H. Mao and A. D. Zhao, Single-atom protecting group for on-surface synthesis of graphdiyne nanowires, *J. Chem. Phys.*, 2019, **32**(5), 620.
56 Z.-F. Cai, N. Kumar and R. Zenobi, Probing On-Surface Chemistry at the Nanoscale Using Tip-Enhanced Raman Spectroscopy, *CCS Chem.*, 2022, **5**(1), 55–71.
57 A. Lucotti, M. Tommasini, M. D. Zoppo, G. Castiglioni, C. Zerbi, F. Cataldo, C. S. Casari, A. L. Bassi, V. Russo, M. Bogana and C. E. Bottani, *Chem. Phys. Lett.*, 2006, **417**, 78–82.
58 L. Talirz, H. Söde, T. Dumslaff, S. Wang, J. R. Sanchez-Valencia, J. Liu, P. Shinde, C. A. Pignedoli, L. Liang, V. Meunier, N. C. Plumb, M. Shi, X. Feng, A. Narita, K. Müllen, R. Fasel and P. Ruffieux, On-Surface Synthesis and Characterization of 9-Atom Wide Armchair Graphene Nanoribbons, *ACS Nano*, 2017, **11**(2), 1380–1388.

59 G. B. Barin, M. Di Giovannantonio, T. G. Lohr, S. Mishra, A. Kinikar, M. L. Perrin, J. Overbeck, M. Calame, X. Feng, R. Fasel and P. Ruffieux, On-Surface Synthesis and Characterization of Teranthene and Hexanthene: Ultrashort Graphene Nanoribbons with Mixed Armchair and Zigzag Edges, *Nanoscale*, 2023, **15**(41), 16766–16774.

60 J. Overbeck, G. B. Barin, C. Daniels, M. L. Perrin, O. Braun, Q. Sun, R. Darawish, M. De Luca, X.-Y. Wang, T. Dumslaff, A. Narita, K. Müllen, P. Ruffieux, V. Meunier, R. Fasel and M. Calame, A Universal Length-Dependent Vibrational Mode in Graphene Nanoribbons, *ACS Nano*, 2019, **13**(11), 13083–13091.

61 R. Darawish, J. Overbeck, K. Müllen, M. Calame, P. Ruffieux, R. Fasel and G. B. Barin, Quantifying Alignment and, Quality of Graphene Nanoribbons: A Polarized Raman Spectroscopy Approach, *Carbon*, 2024, **218**, 118688.

62 G. B. Borin, Q. Sun, M. Di Giovannantonio, C.-Z. Du, X.-Y. Wang, J. P. Llinas, Z. Mutlu, Y. Lin, J. Wilhelm, J. Overbeck, C. Daniels, M. Lamparski, H. Sahabudeen, M. L. Perrin, J. I. Urgel, S. Mishra, A. Kinikar, R. Widmer, S. Stolz, M. Bommert, C. Pignedoli, X. Feng, M. Calame, K. Müllen, A. Narita, V. Meunier, J. Bokor, R. Fasel and P. Ruffieux, Growth Optimization and Device Integration of Narrow-Bandgap Graphene Nanoribbons, *Small*, 2022, **18**(31), e2202301.

63 A. Rabia, F. Tumino, A. Milani, V. Russo, A. L. Bassi, N. Bassi, A. Lucotti, S. Achilli, G. Fratesi, N. Manini, G. Onida, Q. Sun, W. Xu and C. S. Casari, Structural, Electronic, and Vibrational Properties of a Two-Dimensional Graphdiyne like Carbon Nanonetwork Synthesized on Au(111): Implications for the Engineering of sp-sp2 Carbon Nanostructures, *ACS Appl. Nano Mater.*, 2020, **3**, 12178–12187.

64 A. Milani, M. Tommasini, V. Russo, A. L. Bassi, A. Lucotti, F. Cataldo and C. S. Casari, Raman Spectroscopy as a Tool to Investigate the Structure and Electronic Properties of Carbon-Atom Wires, *Beilstein J. Nanotechnol.*, 2015, **6**, 480–491.

65 L. Ravagnan, F. Siviero, C. Lenardi, P. Piseri, E. Barborini, P. Milani, C. Casari, A. L. Bassi and C. Bottani, Cluster-Beam Deposition and in situ Characterization of Carbyne-Rich Carbon Films, *Phys. Rev. Lett.*, 2002, **89**, 285506.

66 F. Cataldo, A Method for Synthesizing Polyynes in Solution, *Carbon*, 2005, **43**, 2792–2800.

67 T. Wakabayashi, H. Tabata, T. Doi, H. Nagayama, K. Okuda, R. Umeda, I. Hisaki, M. Sonoda, Y. Tobo, T. Minematsu, K. Hashimoto and S. Hayashi, Resonance Raman Spectra of Polyyne Molecules C10H2 and C12H2 in Solution, *Chem. Phys. Lett.*, 2007, **433**, 296–300.

68 S. Zhang, J. Wang, Z. Li, R. Zhao, L. Tong, Z. Liu, J. Zhang and Z. Liu, Raman Spectra and Corresponding Strain Effects in Graphyne and Graphdiyne, *J. Phys. Chem. C*, 2016, **120**(19), 10605–10613.

69 J. Zhao and J. Wang, Vibrational and Structural Dynamics of Graphyne, *Int. Rev. Phys. Chem.*, 2022, **41**(3–4), 205–232.

70 A. Basagni, F. Sedona, C. A. Pignedoli, M. Cattelan, L. Nicolas, M. Casarin and M. Sambi, Molecules-Oligomers Nanowires-Graphene Nanoribbons: A Bottom-Up Stepwise On-Surface Covalent Synthesis Preserving Long-Range Order, *J. Am. Chem. Soc.*, 2015, **137**, 1802–1808.

71 F. De Boni, G. Merlin, F. Sedona, S. Casalini, M. M. S. Fakhrabadi and M. Sambi, Templating Effect of Different Low-Miller-Index Gold Surfaces on the Bottom-Up Growth of Graphene Nanoribbons, *ACS Appl. Nano Mater.*, 2020, **3**, 11497–11509.

72 V. V. Ivanovskaya, A. Zobelli, A. Basagni, S. Casalini, L. Colazzo, F. De Boni, D. G. De Oteyza, M. Sambi and F. Sedona, On-Surface Synthesis and Evolution of Self-Assembled Poly (p-phenylene) Chains on Ag (111): A Joint Experimental and Theoretical Study, *J. Phys. Chem. C*, 2022, **127**, 393–402.

73 I. Horcas, R. Fernández, J. M. Gómez-Rodríguez, J. Colchero, J. Gómez-Herrero and A. M. Baro, WSXM: A Software for Scanning Probe Microscopy and a Tool for Nanotechnology, *Rev. Sci. Instrum.*, 2007, **78**, 013705.

74 S. Boker, M. Neale, H. Maes, M. Wilde, M. Spiegel, T. Brick, J. Spies, R. Estabrook, S. Kenny, T. Bates, P. Meht and J. Fox, OpenMx: An Open-Source Extended Structural Equation Modeling Framework, *Psychometrika*, 2011, **76**, 306–317.

75 M. C. Neale, M. D. Hunter, J. N. Pritikin, M. Zahery, T. R. Brick, R. M. Kirkpatrick, R. Estabrook, T. C. Bates, H. H. Maes and S. M. Boker, OpenMx 2.0: Extended Structural Equation and Statistical Modeling, *Psychometrika*, 2016, **81**, 535–549.

76 J. P. Perdew, K. Burke and M. Ernzerhof, Generalized gradient approximation made simple, *Phys. Rev. Lett.*, 1996, **77**, 3865–3868.

77 S. Grimme, Semiempirical GGA-type density functional constructed with a long-range dispersion correction, *J. Comput. Chem.*, 2006, **27**, 1787–1799.

78 J. Tersoff and D. R. Hamann, Theory and Application for the Scanning Tunneling Microscope, *Phys. Rev. Lett.*, 1983, **50**, 1998–2001.

79 J. Ramsey, S. Ranganathan, R. L. McCreery and J. Zhao, Performance comparisons of conventional and line-focused surface Raman spectrometers, *Appl. Spectrosc.*, 2001, **55**, 767–773.

80 M. J. Frisch, G. W. Trucks, H. B. Schlegel, G. E. Scuseria, M. A. Robb, J. R. Cheeseman, G. Scalmani, V. Barone, G. Petersson, H. Nakatsuji, X. Li, M. Caricato, A. Marenich, J. Bloino, B. G. Janesko, R. Gomperts, B. Mennucci, H. P. Hratchian, J. V. Ortiz, A. F. Izmaylov, J. L. Sonnenberg, D. Williams-Young, F. Ding, F. Lipparini, F. Egidi, J. Goings, B. Peng, A. Petrone, T. Henderson, D. Ranasinghe, V. G. Zakrzewski, J. Gao, N. Rega, G. Zheng, W. Liang, M. Hada, M. Ehara, K. Toyota, R. Fukuda, J. Hasegawa, M. Ishida, T. Nakajima, Y. Honda, O. Kitao, H. Nakai, T. Vreven, K. Throssell, J. A. Montgomery, J. Peralta Jr., F. Ogliaro, M. Bearpark, J. J. Heyd, E. Brothers, K. N. Kudin, V. N. Staroverov, T. Keith,

R. Kobayashi, J. Normand, K. Raghavachari, A. Rendell, J. C. Burant, S. S. Iyengar, J. Tomasi, M. Cossi, J. M. Millam, M. Klene, C. Adamo, R. Cammi, J. W. Ochterski, R. L. Martin, K. Morokuma, O. Farkas, J. B. Foresman and D. J. Fox, *Gaussian 09, Revision A.02*, Gaussian, Inc., Wallingford CT, 2016.

81 A. Milani, M. Tommasini and G. Zerbi, Carbynes phonons: A tight binding force field, *J. Chem. Phys.*, 2008, **128**, 064501.

82 T. Wang, H. Lv, J. Huang, H. Shan, L. Feng, Y. Mao, J. Wang, W. Zhang, D. Han, Q. Xu, P. Du, A. Zhao, X. Wu, S. L. Tait and J. Zhu, Reaction selectivity of homochiral versus heterochiral intermolecular reactions of prochiral terminal alkynes on surfaces, *Nat. Commun.*, 2019, **10**, 4122.

83 Y.-Q. Zhang, N. Kepcija, M. Kleinschrodt, K. Diller, S. Fischer, A. C. Papageorgiou, F. Allegretti, J. Bjork, S. Klyatskaya, F. Klappenberger, M. Ruben and J. V. Barth, Homo-Coupling of Terminal Alkynes on a Noble Metal Surface, *Nat. Commun.*, 2012, **3**, 1.

84 K. A. Simonov, N. A. Vinogradov, A. S. Vinogradov, A. V. Generalov, E. M. Zagrebina, N. Mårtensson, A. A. Cafolla, T. Carpy, J. P. Cunniffe and A. B. Preobrajenski, Effect of Substrate Chemistry on the Bottom-Up Fabrication of Graphene Nanoribbons: Combined Core-Level Spectroscopy and STM Study, *J. Phys. Chem. C*, 2014, **118**, 12532–12540.

85 A. Batra, D. Cvetko, G. Kladnik, O. Adak, C. Cardoso, A. Ferretti, D. Prezzi, E. Molinari, A. Morgante and L. Venkataraman, Probing the Mechanism for Graphene Nanoribbon Formation on Gold Surfaces through X-Ray Spectroscopy, *Chem. Sci.*, 2014, **5**, 4419–4423.

86 M. Chen, J. Xiao, H.-P. Steinrück, S. Wang, W. Wang, N. Lin, W. Hieringer and J. M. Gottfried, Combined Photoemission and Scanning Tunneling Microscopy Study of the Surface-Assisted Ullmann Coupling Reaction, *J. Phys. Chem. C*, 2014, **118**, 6820–6830.

87 P. V. Fedotov, D. V. Rybkovskiy, I. V. Novikov and E. D. Obraztsova, Optical Properties of 3-Armchair Graphene Nanoribbons Produced by a Combination of Chemical Vapor Deposition with a Bottom-up Approach, *Phys. Status Solidi B*, 2022, 2100501.

88 E. Mulazzi, A. Ripamonti, J. Wery, B. Dulieu and S. Lefrant, Theoretical and Experimental Investigation of Absorption and Raman Spectra of Poly (paraphenylene vinylene), *Phys. Rev. B: Condens. Matter Mater. Phys.*, 1999, **60**, 16519.